

Low-temperature heat transport of the geometrically frustrated antiferromagnets $R_2\text{Ti}_2\text{O}_7$ ($R = \text{Gd}$ and Er)

F. B. Zhang,¹ Q. J. Li,^{1,2} Z. Y. Zhao,¹ C. Fan,¹ S. J. Li,¹ X. G. Liu,¹ X. Zhao,^{3,*} and X. F. Sun^{1,†}

¹*Hefei National Laboratory for Physical Sciences at Microscale,
University of Science and Technology of China, Hefei, Anhui 230026, People's Republic of China*

²*School of Physics and Material Sciences, Anhui University,
Hefei, Anhui 230601, People's Republic of China*

³*School of Physical Sciences, University of Science and Technology of China,
Hefei, Anhui 230026, People's Republic of China*

(Dated: July 6, 2018)

We report a systematic study on the low-temperature thermal conductivity (κ) of $R_2\text{Ti}_2\text{O}_7$ ($R = \text{Gd}$ and Er) single crystals with different directions of magnetic field and heat current. It is found that the magnetic excitations mainly act as phonon scatterers rather than heat carriers, although these two materials have long-range magnetic orders at low temperatures. The low- T $\kappa(H)$ isotherms of both compounds show rather complicated behaviors and have good correspondences with the magnetic transitions, where the $\kappa(H)$ curves show drastic dip- or step-like changes. In comparison, the field dependencies of κ are more complicated in $\text{Gd}_2\text{Ti}_2\text{O}_7$, due to the complexity of its low- T phase diagram and field-induced magnetic transitions. These results demonstrate the significant coupling between spins and phonons in these materials and the ability of heat-transport properties probing the magnetic transitions.

PACS numbers: 66.70.-f, 75.47.-m, 75.50.-y

I. INTRODUCTION

Geometrically frustrated antiferromagnets have been a topic of significant interest due to their abundant and exotic physical properties.^{1–5} The rare-earth titanates $R_2\text{Ti}_2\text{O}_7$ ($R = \text{rare earth}$) are one of the families with three-dimensional spin frustration.^{4,5} These materials have pyrochlore crystal structure with the space group $Fd\bar{3}m$, in which the magnetic rare-earth ions form a network of corner-sharing tetrahedra and are prone to a high degree of geometric frustration. For this reason, antiferromagnetically coupled classical Heisenberg spins on the pyrochlore lattice cannot form a long-range order at finite temperature. However, the real materials are greatly sensitive to weak perturbations (e.g. single-ion anisotropy, dipolar interaction or quantum fluctuations) beyond the nearest-neighboring exchange, which results in rich unconventional low-temperature magnetic and thermodynamic properties. Example phenomena include the disordered classical spin ice in $\text{Ho}_2\text{Ti}_2\text{O}_7$ and $\text{Dy}_2\text{Ti}_2\text{O}_7$ (with effective ferromagnetic exchange and Ising anisotropy),^{6,7} the quantum spin liquid in $\text{Tb}_2\text{Ti}_2\text{O}_7$,^{8–10} and the quantum spin ice in $\text{Yb}_2\text{Ti}_2\text{O}_7$.^{11,12} Furthermore, the long-range antiferromagnetic (AF) order can be formed in $\text{Gd}_2\text{Ti}_2\text{O}_7$ and $\text{Er}_2\text{Ti}_2\text{O}_7$.^{13,14} Recently, the low- T heat transport properties of $R_2\text{Ti}_2\text{O}_7$ have started to attract research interests for the purpose of detecting the transport of magnetic excitations in these materials. The spin-ice compounds exhibit considerably strong interactions between the magnetic excitations and phonons and hence show drastic changes of thermal conductivity at the field-induced magnetic transitions.^{15–17} In the spin-liquid material $\text{Tb}_2\text{Ti}_2\text{O}_7$, the coupling between spin fluctuations and phonons is so strong that the phonon heat transport

is extremely weak.¹⁸ In this work, we study the low- T thermal conductivity of two long-range ordered systems $R_2\text{Ti}_2\text{O}_7$ ($R = \text{Gd}$ and Er) to probe the roles of magnon excitations and magnetic fluctuations.

In $\text{Gd}_2\text{Ti}_2\text{O}_7$, the magnetic Gd^{3+} ion has a spin momentum $S = 7/2$ and an orbital momentum $L = 0$, and therefore has a negligible single-ion anisotropy.¹³ In zero field, $\text{Gd}_2\text{Ti}_2\text{O}_7$ shows the magnetic-order transition induced by thermal fluctuation at about 1 K to the so-called P state.^{19–23} Lowering temperature to about 0.7 K, the P state changes to a so-called F state. It was found that both P and F states have a specific $4-k$ magnetic structure with $\mathbf{k} = (1/2, 1/2, 1/2)$, in which all the Gd^{3+} spins are perpendicular to the local $[111]$ axes.¹⁹ However, in the F state each pyrochlore unit cell consists of three fully ordered spin tetrahedra and one weakly ordered spin tetrahedron, while in the P state that weakly ordered spin tetrahedron becomes fully disordered.¹⁹ With applying magnetic field, the Gd^{3+} spin structures present further changes.^{24–28} At $H \geq 3$ T and $T < 1$ K, a collinear spin state is formed, in which three spins on each tetrahedron are aligned with the field and the rest one points to the opposite direction.²⁵ In high magnetic fields, the Gd^{3+} spins enter a polarized paramagnetic state. The mechanisms of these field-driven transitions are likely that magnetic field can break the degenerate ground states and force the system to select a particular ordered structure.

$\text{Er}_2\text{Ti}_2\text{O}_7$ was proposed to be a realization of the XY antiferromagnet on pyrochlore lattice. Er^{3+} ion has a large orbital momentum $L = 6$ and a spin momentum $S = 3/2$. However, the crystal-field ground state of Er^{3+} ion is a Kramers doublet, with large anisotropy respective to the local $[111]$ axis, and can be described as an effec-

tive spin of $1/2$.^{14,29} This implies a significant quantum effect in this material. $\text{Er}_2\text{Ti}_2\text{O}_7$ undergoes a second-order transition to a long-range ordered state at about 1.2 K with an unusual $\mathbf{k} = 0$ non-coplanar AF structure, the so-called ψ_2 state.^{14,29–35} The mechanism of this long-range ordered phenomenon had been discussed to be the quantum order by disorder effect,^{32,36} for which the quantum fluctuations lift the degeneracy of the ground state. Applying magnetic field above a critical value of 1.5–2 T (slightly different for $H \parallel [100]$, $[110]$, and $[111]$), the system enters a high-field quantum paramagnetic state through a second-order transition driven by the quantum fluctuations. In the high-field state, the Er^{3+} spins are fully polarized in the XY plane and maximize their projections along the field direction.^{30,35,37}

Both $\text{Gd}_2\text{Ti}_2\text{O}_7$ and $\text{Er}_2\text{Ti}_2\text{O}_7$ exhibit the ground states of a coexistence of the long-range order and short-range order or spin fluctuations,^{14,30,38,39} which are obviously different from the conventional magnetic materials. One can naturally expect that their heat transport properties would show some peculiar phenomena. In this paper, we perform detailed studies of the low- T thermal conductivity of $R_2\text{Ti}_2\text{O}_7$ ($R = \text{Gd}$ and Er) single crystals and find that they have rather complicated temperature and magnetic-field dependencies. To probe the mechanism of the heat transport properties, the low- T specific heat are also studied. The data demonstrate that the magnetic excitations in these materials can effectively scatter phonons instead of transport heat. Due to the spin-phonon coupling, the field-induced phase transitions cause drastic changes of the phonon thermal conductivity.

II. EXPERIMENTS

High-quality $R_2\text{Ti}_2\text{O}_7$ ($R = \text{Gd}$ and Er) single crystals were grown using a floating-zone technique.⁴⁰ In particular, $\text{Gd}_2\text{Ti}_2\text{O}_7$ and $\text{Er}_2\text{Ti}_2\text{O}_7$ were grown in 0.4 MPa pure oxygen with a growth rate of 2.5 mm/h and in 0.1 MPa pure oxygen with a rate of 4 mm/h, respectively. The crystals were oriented by the x-ray Laue photograph and cut precisely along those crystallographic axes like $[111]$, $[110]$ (or $[1\bar{1}0]$), and $[11\bar{2}]$ into long-bar and thin-plate shapes for the thermal conductivity and specific heat measurements, respectively. The thermal conductivity was measured at low temperatures down to 0.3 K and in magnetic fields up to 14 T by using a conventional steady-state technique.^{15,18,41–45} The specific heat was measured at low temperatures down to 0.4 K by using the relaxation method in a commercial physical property measurement system (PPMS, Quantum Design).

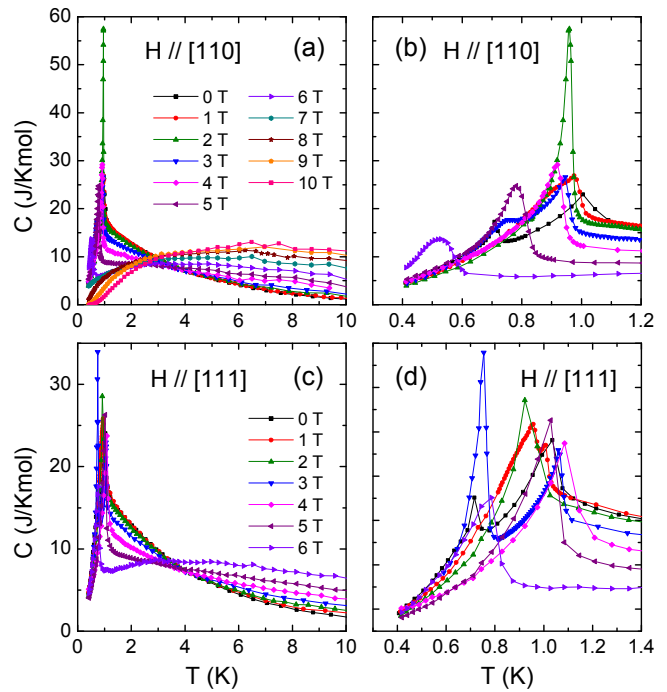


FIG. 1: (Color online) (a,c) Temperature dependencies of the specific heat of $\text{Gd}_2\text{Ti}_2\text{O}_7$ single crystals for $H \parallel [110]$ and $H \parallel [111]$. (b,d) Zoom-in of the low-temperature plots. The sample sizes are $0.29 \times 0.32 \times 0.17 \text{ mm}^3$ for $H \parallel [110]$ and $0.53 \times 0.53 \times 0.09 \text{ mm}^3$ for $H \parallel [111]$, respectively. The magnetic fields were applied along the shortest dimensions of the samples.

III. RESULTS

A. $\text{Gd}_2\text{Ti}_2\text{O}_7$

Figure 1 shows the low- T specific heat data of $\text{Gd}_2\text{Ti}_2\text{O}_7$ single crystals for $H \parallel [110]$ and $H \parallel [111]$. In zero magnetic field, there are two peaks at 1.0 and 0.71 K, which represent two consecutive transitions from paramagnetic state to the P state and then to the F state, respectively. In applied fields along the $[110]$ direction, the two peaks merge with each other and a broad peak can be seen at 1 T. Increasing field to 2 T, the peak becomes much larger and a bit sharper and is locating at 0.96 K. However, this peak splits into a peak at 0.95 K and a lower shoulder at 0.77 K when magnetic field is increased to 3 T. Increasing field further to 4 T, the peak shifts to 0.92 K while the shoulder-like feature disappears. For $H > 4$ T, the remained peak gradually moves to lower temperatures and cannot be seen at temperature down to 0.4 K when the field is larger than 6 T. Finally, a hump-like feature appears and gradually shifts to high temperatures for $H > 6$ T. It resembles a Schottky anomaly and is apparently related to the Zeeman effect of the Gd^{3+} moments in the high-field paramagnetic state. All these phenomena are essentially consistent with the results reported previously,^{20,24,25} which

were discussed to originate from the partial lift of degenerate states.²⁴ The specific-heat data in $H \parallel [111]$ show rather similar behaviors to those in $H \parallel [110]$, but with some obvious differences in the positions and magnitudes of those peaks, which indicates a non-negligible magnetic anisotropy of $\text{Gd}_2\text{Ti}_2\text{O}_7$.^{21,25,46}

Figures 2(a)-2(c) show the thermal conductivity as a function of temperature in zero and 14 T fields for different directions of magnetic field and heat current (J_H). Apparently, the heat transport of $\text{Gd}_2\text{Ti}_2\text{O}_7$ is almost isotropic in both zero and 14 T fields and is independent of the field direction. The zero-field $\kappa(T)$ curves exhibit a typical phonon transport behavior at high temperatures and large phonon peaks at about 10 K.⁴⁷ It is notable that at the phase transitions from the high- T paramagnetic state to the low- T magnetically ordered state at 1.0 and 0.7 K, indicated by the specific-heat data, there is no obvious change of $\kappa(T)$. It seems that the magnetic excitations of $\text{Gd}_2\text{Ti}_2\text{O}_7$ have no obvious contribution to transporting heat. However, at low temperatures the κ is increased in 14 T, indicating that there is magnetic scattering on phonons in zero field that can be removed by applying high field.⁴²

The detailed magnetic-field dependencies of the low- T thermal conductivities are shown in Figs. 2(d)-2(f). For three different configurations, $\kappa(H)$ isotherms show very similar behaviors. At very low temperatures, the κ shows some reduction at low fields, a step-like increase at about 6 T, and a high-field plateau. Upon increasing temperature, the low-field reduction is weakened and the transition at 6 T is broadened, accompanied with a decrease of the high-field plateau. At 1.95 K, the κ is almost independent of field. At lowest temperature, the high-field plateau is started from 7–8 T. From the specific-heat data, it is known that above 8 T the samples enter the paramagnetic or the high-field polarized state. Therefore, the step-like increase and high-field plateau of κ are apparently originated from the quench of the phonon scattering by magnetic excitations (magnons from the ordered state), when entering the spin-polarized state.⁴² This means that the low- T thermal conductivity in high fields would be a phonon transport free from magnetic scattering. However, one may note that at sub-Kelvin temperatures the 14-T $\kappa(T)$ curves have some obvious curvatures in the log-log plot instead of showing a power law close to T^3 . It is deviated from the expectation of a phonon heat transport in the boundary scattering limit.⁴⁷ This unusual temperature dependence points to some peculiarity of the high-field magnetic state of $\text{Gd}_2\text{Ti}_2\text{O}_7$. Nevertheless, it is rather clear that magnons in this material mainly play a role of scattering phonons and there is no signature that they can contribute substantially to transporting heat.

It can also be seen that the low-field behaviors of $\kappa(H)$ are a bit different for three different configurations of heat current vs field direction. For $H \parallel [111]$, as shown in Fig. 2(d), the 0.36-K $\kappa(H)$ curve has two pronounced “dips” at 1 and 3.25 T. With increasing temperature, they be-

come more shallow and disappear above 1 K. For $H \parallel [110]$ (or $\perp [111]$), as shown in Figs. 2(e) and 2(f), the 0.36-K $\kappa(H)$ curves show two weak “dips”, which are slightly different between $J_H \parallel [111]$ and $J_H \parallel [110]$. In the former case, they locate at about 1 and 3.5 T, while in the latter case they locate at about 1 and 3 T (the 1 T dip in Fig. 2(f) is very weak). Note that in these cases, the relative directions between the heat current and magnetic field are different, which yields some difference in the demagnetization effect. Considering this factor, the positions of two dips depend on the direction of magnetic field rather than that of heat current. These two dips disappear quickly with increasing temperature.

It should be noted that these low- T $\kappa(H)$ isotherms do not display obvious hysteresis, which indicates that the possible magnetic domains²⁸ are not coupled with the phonon transport. In this regard, the $\kappa(H)$ results are not able to distinguish the order of phase transition at 6 T, which either a weak first-order transition or a second-order one were suggested by some earlier experimental results.^{25,48}

To probe the origin of the $\kappa(H)$ behaviors, we compare the characteristic fields, including the dips and step-like increase, with those transitions from the specific-heat data. In Fig. 3, the $H - T$ phase diagrams of $\text{Gd}_2\text{Ti}_2\text{O}_7$ for either $H \parallel [111]$ or $H \parallel [110]$ are determined by the transitions from the specific heat. They are nearly the same as those in some earlier literature.²⁵ It is known that there are at least four different magnetic phases in the phase diagram, that is, the high- T and high-field paramagnetic (PM) phase, the low- T and low-field F state, a lower-field P state, and a higher-field collinear state (see the Introduction section). It is found that the characteristic fields from the $\kappa(H)$ data have a good correspondence with the phase boundaries among these four phases. The step-like increase of κ at about 6 T is caused by the transition from the low-field ordered state to the paramagnetic state.⁴² It can be explained as the elimination of the magnon scattering on phonons in a spin-polarized state. The dip of $\kappa(H)$ at about 3 T is caused by the transition from the F state to the collinear state. It seems that this transition is a rearrangement of the spin structure, which is usually associated with the collapse of the spin anisotropy gap and the increased numbers of low-energy magnons. The phonon scattering is enhanced by a large number of magnons at the transition fields.^{42–44} Another dip of κ at about 1 T, however, has no direct relationship to the specific-heat data. In the phase diagrams determined by the specific heat, this transition is locating deeply in the F state. In this regard, it may be related to a very recent experimental finding of a new phase boundary at 1 T for $H \parallel [100]$.²⁸ This boundary separates some unknown phases (named as I and I' in Ref. 28) from the F state. Since the phase diagrams of $\text{Gd}_2\text{Ti}_2\text{O}_7$ are rather similar for different field directions,²⁵ it is reasonable to believe that these newly found phases and phase boundaries exist also in the cases of $H \parallel [111]$ and $H \parallel [110]$. Finally, it should

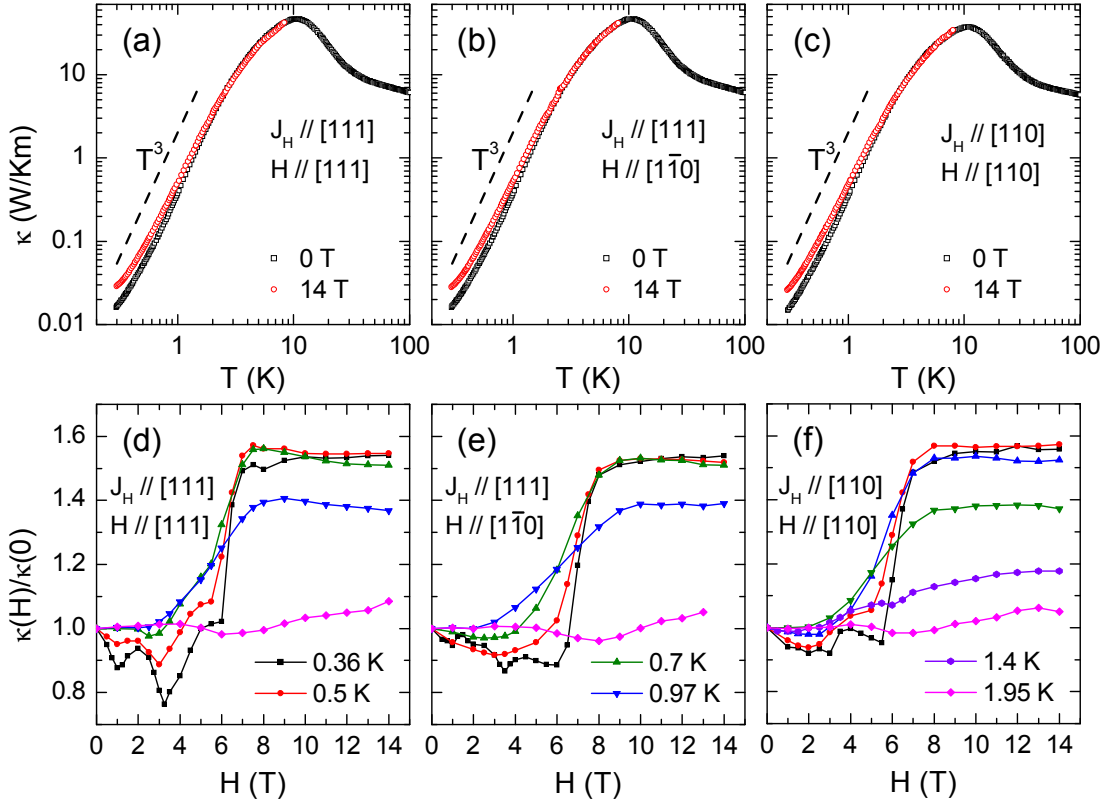


FIG. 2: (Color online) (a-c) Temperature dependencies of thermal conductivities of $\text{Gd}_2\text{Ti}_2\text{O}_7$ single crystals in zero and 14 T. The directions of heat current (J_H) and magnetic field are along either the [111] or the [110] directions. Note that in panel (b), the magnetic fields along the $[1\bar{1}0]$ direction (equivalent to the [110]) are actually perpendicular to the [111] direction. The dashed lines indicate a T^3 temperature dependence. (d-f) The corresponding magnetic-field dependencies of thermal conductivities at low temperatures for the three different configurations. Two sets of data for $J_H \parallel [111]$ were taken on a sample having a size of $3.9 \times 0.63 \times 0.17 \text{ mm}^3$. Another sample for $J_H \parallel [110]$ has a size of $2.4 \times 0.65 \times 0.16 \text{ mm}^3$. The heat currents were flowing along the longest dimensions of these samples.

be pointed out that the small differences in the critical fields between the $\kappa(H)$ data and the specific-heat data are probably due to either the uncertainty in defining the transition fields in two different physical properties or the difference in the demagnetization effect, or both.

B. $\text{Er}_2\text{Ti}_2\text{O}_7$

Figure 4(a) shows the low- T specific heat of $\text{Er}_2\text{Ti}_2\text{O}_7$ single crystal. In zero field, a sharp λ peak appears at about 1.2 K, which reveals a second-order phase transition from the paramagnetic state to the long-range ordered state. Applying magnetic field along the [111] direction, the peak is gradually suppressed and shifts to lower temperatures. It is not observable at temperatures down to 0.4 K with $H \geq 2$ T. At the same time, a much broader peak emerges at about 1.3 K when $H = 1.5$ T. It shifts to higher temperatures and becomes even broader with increasing field, which behaves like a Schottky anomaly.^{30,31} All these are in good agreement with the previous results.^{14,30,31} In literatures, the specific

heat of $\text{Er}_2\text{Ti}_2\text{O}_7$ were studied for three different directions of magnetic field, that is, $H \parallel [100]$, $[110]$, and $[111]$, and were found to show some anisotropy of the transition fields between the ground state and the high-field quantum paramagnetic state. Furthermore, the high-field specific heat were dependent on the field direction. In particular, the high-field humps or broad peaks in the [100] and [110] fields could be described by a simple two-level Schottky anomaly, while those in the [111] fields could not.³¹ Our present data confirmed this. As shown in Fig. 4(b), the high-field data ($H \geq 2$ T) are fitted using the following formula

$$C = \alpha R \left(\frac{\Delta}{k_B T} \right)^2 \frac{e^{-\Delta/k_B T}}{(1 + e^{-\Delta/k_B T})^2} + \beta T^3, \quad (1)$$

where the first term represents the two-level Schottky anomaly and the second one is the phonon contribution. Here, R is the universal gas constant, α is a numerical coefficient, Δ is the gap value and is dependent on the Zeeman effect, and β is the coefficient for low- T phonon specific heat. It is found that this formula could qualitatively describe the data but the fittings are not perfect,

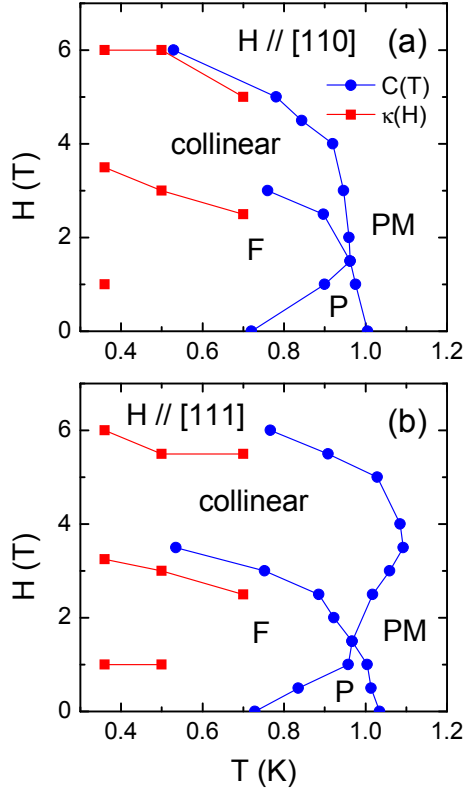


FIG. 3: (Color online) Temperature-field phase diagrams of $\text{Gd}_2\text{Ti}_2\text{O}_7$ single crystals obtained from the specific-heat data for $H \parallel [110]$ and $H \parallel [111]$. The characteristic fields of the $\kappa(H)$ curves are also plotted for the comparison. PM is the high-temperature paramagnetic state. The P , F , and collinear states are three different phases mentioned in the main text.

which is very similar to the earlier study by Sosin *et al.*³¹ Note that the parameters in our fittings, $\alpha = 1.65$ and $\beta = 2.8 \times 10^{-3} \text{ J/K}^4\text{mol}$, are also almost the same as those in Ref. 31. All these indicate that for $H \parallel [111]$, higher-field Schottky-like peaks are not a simple behavior of paramagnetic moments. Some soft modes related to the spin fluctuations are probably involved.^{30,31}

In a theoretical scenario, $\text{Er}_2\text{Ti}_2\text{O}_7$ was found to have a ground state of quantum order by disorder and exhibit a quantum critical point at 1.5–2 T, where the long-range order is suppressed.^{31–33} However, the zero-field long-range order actually coexists with spin fluctuations, as revealed by the magnetic resonance spectroscopy and inelastic neutron scattering.^{30,31} These soft spin excitations would not only contribute to the specific heat but also be easily coupled with low-energy phonons and significantly damp the phonon transport.¹⁸ Across the quantum critical field (1.5–2 T), the magnetic excitations of ground state change drastically, which in principle could be detected by the thermal conductivity.

Figure 5 shows the temperature and magnetic-field dependencies of the thermal conductivity for different directions of heat current and magnetic field. Both the $\kappa(T)$

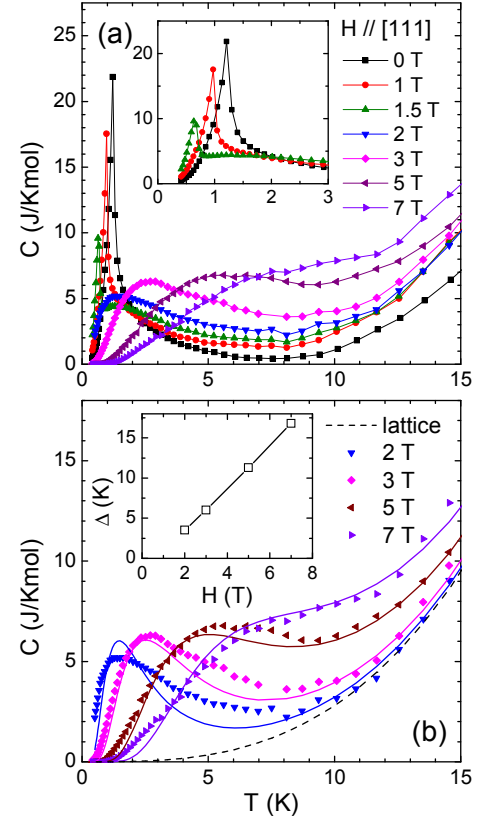


FIG. 4: (Color online) (a) Temperature dependencies of the specific heat of $\text{Er}_2\text{Ti}_2\text{O}_7$ single crystal for magnetic field along the $[111]$ axis. Inset: Zoom-in of the low-temperature plot. The sample size is $0.46 \times 0.67 \times 0.08 \text{ mm}^3$, with the field direction along the shortest dimension. (b) The fits of the high-field data ($H \geq 2 \text{ T}$) to Eq. (1) as described in the main text. The solid lines represent the fitting results and the dashed line shows the phonon contribution. Inset displays the fitting parameter Δ .

curves and the low- T $\kappa(H)$ isotherms show no obvious anisotropy. As far as the zero-field $\kappa(T)$ data are concerned, the phonon peaks locate at about 8 K; below about 1.2 K, as shown in the inset to Fig. 5(c), some slight changes in the slopes of these $\kappa(T)$ can be seen, which is related to the phase transition from the paramagnetic state to the long-range ordered state. With applying field of 1.5 or 2 T, the κ become much smaller than the zero-field data and the changes of the $\kappa(T)$ slopes at $\sim 1.2 \text{ K}$ are more significant. In a high field of 14 T, the κ values are larger than the zero-field values at low temperatures, which indicates that in the spin-polarized state, the phonon scattering by magnetic excitations is quenched and the phonon transport is recovered. However, at relatively higher temperatures, the κ in 14 T field is much smaller than the zero-field value, suggesting a field-induced magnetic scattering effect. This is different from the high- T behavior of $\text{Gd}_2\text{Ti}_2\text{O}_7$.

The $\kappa(H)$ isotherms show a dip-like behavior at low fields and an increase at high fields, particularly at very

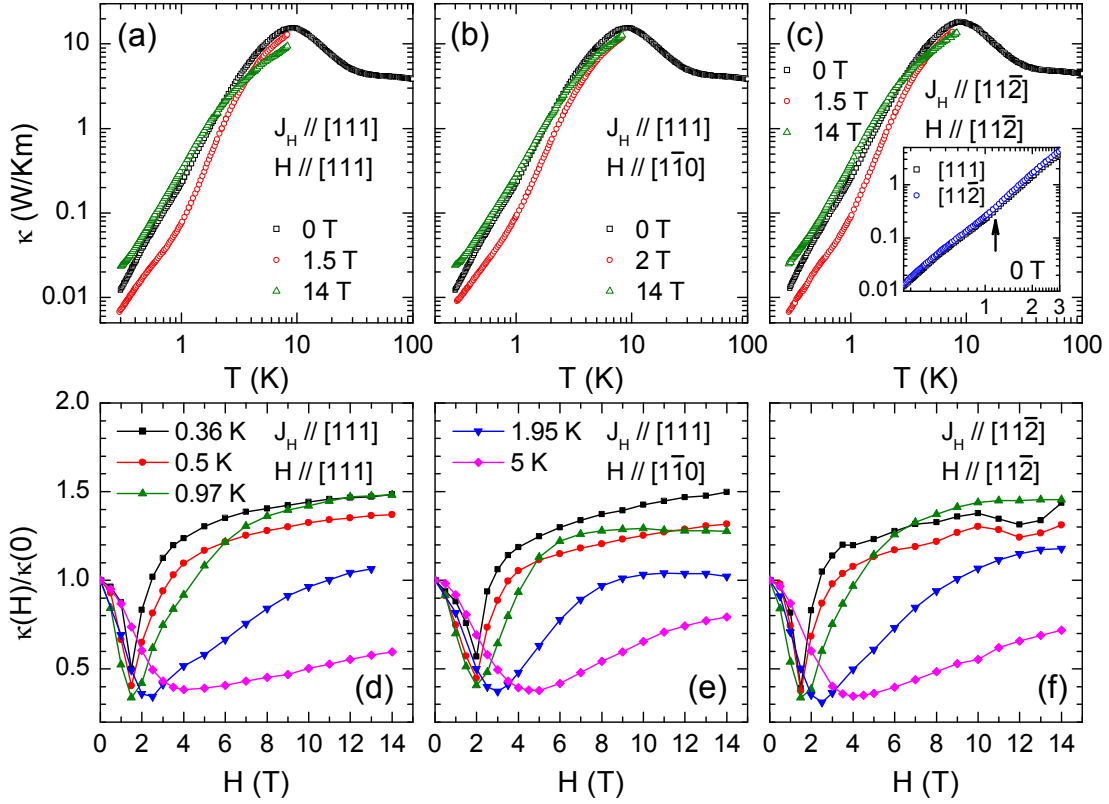


FIG. 5: (Color online) (a-c) Temperature dependencies of thermal conductivities of $\text{Er}_2\text{Ti}_2\text{O}_7$ single crystals for different directions of heat current (J_H) and magnetic field. In panel (b), the magnetic fields along the $[1\bar{1}0]$ (equivalent to the $[110]$) are actually perpendicular to the $[111]$ direction. In panel (c), both the heat current and the magnetic fields are along the $[11\bar{2}]$ direction, which is actually perpendicular to the $[111]$ axis. The inset to panel (c) shows the zoom in of the zero-field $\kappa(T)$ curves in temperature regime of 0.3–3 K, and the arrow indicates a weak change in slopes of these data. (d-f) The corresponding magnetic-field dependencies of thermal conductivities at low temperatures for the three different configurations. The sample sizes are $3.4 \times 0.65 \times 0.17 \text{ mm}^3$ for $J_H \parallel [111]$ and $4.0 \times 0.65 \times 0.18 \text{ mm}^3$ for $J_H \perp [111]$, respectively. The heat currents were flowing along the longest dimensions of them.

low temperatures. At the first glance, it is similar to that caused by paramagnetic scattering on phonons.^{45,49,50} But one may note a remarkable difference between the $\text{Er}_2\text{Ti}_2\text{O}_7$ results and the paramagnetic scattering phenomenon. In the latter case, the minimum or dip of the $\kappa(H)$ isotherm is due to a phonon resonant scattering by some magnetic excitations between the energy levels that are affected by the Zeeman effect,^{45,47,49,50} therefore, the position of the dip should shift almost linearly with the magnetic field. For $\text{Er}_2\text{Ti}_2\text{O}_7$, at higher temperatures ($> 1 \text{ K}$), the dip of κ becomes broader and shifts to higher fields with increasing temperature, which is indeed the same as the paramagnetic scattering effect. However, as can be seen in Figs. 5(d)-5(f), the dip fields are temperature independent for $T < 1 \text{ K}$. Apparently, this sub-Kelvin behavior must have some other origin. Since the low- T dip fields (1.5 or 2 T) are close to the characteristic field in the specific heat, above which the λ peak was suppressed, it is likely that they correspond to the phase transition from the low-field ordered state to the high-field quantum paramagnetic state. In passing, it should be pointed out that the dip field is essentially

isotropic for different field directions, as shown by Figs. 5(d) and 5(f), while the higher dip fields in Fig. 5(e) could be due to the demagnetization effect. In addition, the $\kappa(H)$ curves at 0.36 and 0.5 K in Fig. 5(f) display shallow minimums at high field ($> 10 \text{ T}$). It is unclear whether they are related to some kind of transition since the feature is rather weak and broad.

Figure 6 shows the comparison of dip fields of the $\kappa(H)$ with the characteristic fields of the specific heat. It is clear that the dips of $\kappa(H)$ have no good correspondence with the phase boundary of the AF state, and at different temperature regions they have very different origins. At very low temperatures ($T < 1 \text{ K}$), the dips are coincided with the quantum critical field that suppresses the long-range-ordered ground state, which can be ascribed to be a simple explanation of the strong phonon scattering by the critical magnetic fluctuations. This is supported by a complete mode softening of spin excitations at H_c as revealed by the inelastic neutron scattering.³⁰ The higher-field enhancement of κ is due to the removal of low-lying magnetic excitations at $H > H_c$.³⁰ On the other hand, the higher- T ($T > 1 \text{ K}$) dips have a good correspon-

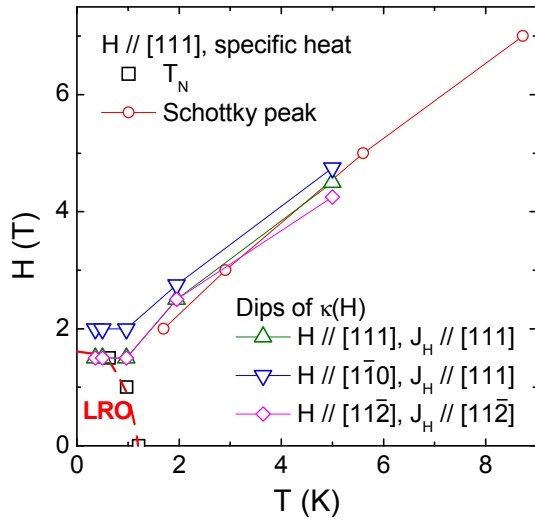


FIG. 6: (Color online) Temperature-field phase diagram of $\text{Er}_2\text{Ti}_2\text{O}_7$ single crystal for $H \parallel [111]$ from the specific-heat data. The low- T λ peak gives the antiferromagnetic transition temperature T_N . The field dependence of T_N displays the phase boundary of the long-range ordered (LRO) ground state, as shown by the dashed line. The higher-field Schottky-like peaks may separate the “high- T , low-field” thermally paramagnetic state and the “high-field, low- T ” quantum paramagnetic state, as suggested by Ref. 30. The characteristic dip fields of the $\kappa(H)$ isotherms are also shown for three configurations of the heat current (J_H) and magnetic field.

dence with the higher-field Schottky-like anomalies of the specific heat. Although this anomaly was discussed to separate the “high- T , low-field” thermally paramagnetic state and the “high-field, low- T ” quantum paramagnetic state,³⁰ the paramagnetic excitations are the main contribution and are likely playing a role of scattering phonon. Therefore, it is understandable that the $\kappa(H)$ behaviors at $T > 1$ K match well with the phonon resonant scattering effect by the paramagnetic ions.

IV. DISCUSSION

Both $\text{Gd}_2\text{Ti}_2\text{O}_7$ and $\text{Er}_2\text{Ti}_2\text{O}_7$ display the magnetic excitations scattering on phonons. It seems to be a common phenomenon in pyrochlore $R_2\text{Ti}_2\text{O}_7$. In spin-ice members $\text{Dy}_2\text{Ti}_2\text{O}_7$ and $\text{Ho}_2\text{Ti}_2\text{O}_7$, there is negligible scattering on phonons by the magnetic excitations in zero field.^{15–17} This is due to the fact that the peculiar magnetic excitations, magnetic monopoles, in the spin-ice compounds have sizeable energy gaps that prevent the thermal activations at very low temperatures.⁵¹ However, in magnetic fields the magnetic monopoles can be well populated and were found to scatter phonons rather strongly, particularly at the field-induced magnetic transitions between the “spin-ice”, the “kagomé-ice”, and the “three-in-one-out” states, although they might be able to

transport heat also.^{15–17} In the quantum-spin-liquid material $\text{Tb}_2\text{Ti}_2\text{O}_7$, the coupling between spin fluctuations and phonons is so strong that the phonon heat transport exhibits a glassy-like behavior.¹⁸ In comparison, the coupling or scattering effect between magnetic excitations and phonons in the long-range ordered $\text{Gd}_2\text{Ti}_2\text{O}_7$ and $\text{Er}_2\text{Ti}_2\text{O}_7$ are not very strong but detectable at zero field.

One reason that the magnetic excitations act mainly as phonon scatterers rather than heat carriers in $R_2\text{Ti}_2\text{O}_7$ is apparently related to the rather weak exchange interactions in these materials. As a result, the magnetic excitations have weak dispersion or small velocity. An example is that the magnetic monopoles in the spin-ice compounds were estimated to have a small velocity of ~ 20 m/s.¹⁶ The magnon velocity of $\text{Er}_2\text{Ti}_2\text{O}_7$, calculated from the dispersion curve, is about 80 m/s only.²⁹ $\text{Gd}_2\text{Ti}_2\text{O}_7$ is expected to have a similar situation, since the exchange energies of these materials are essentially comparable.^{13,29,35,38} In contrast, the magnon velocity is about 2–4 orders of magnitude larger in many materials that show substantial magnon heat transport.^{52–54}

Although the heat transport of $\text{Gd}_2\text{Ti}_2\text{O}_7$ and $\text{Er}_2\text{Ti}_2\text{O}_7$ have some similarities in the weak anisotropy and magnetic scattering effect, there are several notable differences between them. First, $\text{Gd}_2\text{Ti}_2\text{O}_7$ shows much larger phonon peaks in the zero-field $\kappa(T)$ curves, even though these two compounds have the same crystal structures. For nonmagnetic insulators, larger phonon peak may indicate less structural imperfections in crystals. However, for magnetic materials, the magnetic scattering can play a role. This possibility seems to be supported by the details of the temperature dependence of κ . As can be seen in Figs. 2 and 5, near the long-range order transition in zero field, the $\kappa(T)$ of $\text{Gd}_2\text{Ti}_2\text{O}_7$ do not show any observable changes, while those of $\text{Er}_2\text{Ti}_2\text{O}_7$ show weak changes of the $\kappa(T)$ slopes. Second, the magnetic scatterings actually have quite different origins in these two materials. In $\text{Gd}_2\text{Ti}_2\text{O}_7$, the magnetic excitations of the long-range ordered state, *i.e.*, magnons are effectively phonon scatterers. For this reason, the magnetic-field-induced changes of κ are only presented at low temperatures; above 2 K, the κ is nearly unaffected by applying field. In $\text{Er}_2\text{Ti}_2\text{O}_7$, however, the role of magnons in the long-range ordered state is not so obvious. Nevertheless, in zero field and at very low temperatures, magnons are likely to scatter phonons, since the high-field κ are about 50% larger than the zero-field values. On the other hand, the low-energy spin excitations associated with the quantum critical point induce a strong scattering on phonons in a rather broad temperature range. Another contribution of the magnetic excitations is the high- T paramagnetic scattering effect. In this regard, it is rather difficult to understand why there is no any signature of paramagnetic scattering effect in $\text{Gd}_2\text{Ti}_2\text{O}_7$. Third, $\text{Gd}_2\text{Ti}_2\text{O}_7$ shows much more complicated $\kappa(H)$ behaviors than $\text{Er}_2\text{Ti}_2\text{O}_7$. This is clearly due to a more complicated low- T phase diagram of $\text{Gd}_2\text{Ti}_2\text{O}_7$. In present work, the low- T heat transport of these materials again

shows a close relationship to the magnetism and magnetic transitions, as also found in many other magnetic materials.^{15,16,41–44} It therefore provides a useful tool to probe some unknown magnetic transitions, as shown in Fig. 3.

There are also some details remained to be further studied. As shown in Fig. 2, the temperature dependencies of κ of $\text{Gd}_2\text{Ti}_2\text{O}_7$ show some clear deviations from the power law at sub-Kelvin temperatures even in 14 T field. This may suggest that the magnetic scattering in the high-field spin-polarized state is still active at such low temperatures. This unusual temperature dependence points to some peculiarity of the high-field magnetic state of $\text{Gd}_2\text{Ti}_2\text{O}_7$. One possible reason is that the ground state of $\text{Gd}_2\text{Ti}_2\text{O}_7$ is a coexisting of long-range and short-ranges orders. The short-range order or spin fluctuations could survive in high field even when the long-range AF order was suppressed. A supportive experimental result is that the magnetic resonance spectroscopy has detected some weakly dispersive soft modes in the spin-saturated phase, which could be explained based on the spin-wave calculations.²⁷

V. SUMMARY

Thermal conductivities of pyrochlore $R_2\text{Ti}_2\text{O}_7$ ($R = \text{Gd}$ and Er) are studied at low temperatures down to 0.3

K and in high fields up to 14 T. It is found that the magnetic excitations play a role of scattering phonons rather than transporting heat, although these two materials have long-range magnetic orders at low temperatures. In $\text{Gd}_2\text{Ti}_2\text{O}_7$, the field-induced magnetic transitions can cause drastic changes of κ at the phase boundaries and lead to rather complicated field dependencies of κ . The main phenomena include the dip-like features in $\kappa(H)$ isotherms at the low-field phase transitions and a step-like increase of κ at the spin-polarization transition. $\text{Er}_2\text{Ti}_2\text{O}_7$ shows much simpler field dependencies of κ , with a dip-like feature caused by the quantum phase transition at about 1.5–2 T or the paramagnetic phonon scattering at higher temperatures. These data demonstrate that heat transport is an effective means to probe the magnetic properties of pyrochlore rare-earth titanates.

Acknowledgments

This work was supported by the National Natural Science Foundation of China, the National Basic Research Program of China (Grants No. 2009CB929502 and No. 2011CBA00111), and the Fundamental Research Funds for the Central Universities (Program No. WK2340000035).

* Electronic address: xiazhao@ustc.edu.cn

† Electronic address: xfsun@ustc.edu.cn

¹ P. Schiffer and A. P. Ramirez, *Comments Condens. Matter Phys.* **18**, 21 (1996).

² P. Lecheminant, B. Bernu, C. Lhuillier, L. Pierre, and P. Sindzingre, *Phys. Rev. B* **56**, 2521 (1997).

³ F. Mila, *Phys. Rev. Lett.* **81**, 2356 (1998).

⁴ B. Canals and C. Lacroix, *Phys. Rev. Lett.* **80**, 2933 (1998).

⁵ J. S. Gardner, M. J. P. Gingras, and J. E. Greedan, *Rev. Mod. Phys.* **82**, 53 (2010).

⁶ S. T. Bramwell and M. J. P. Gingras, *Science* **294**, 1495 (2001).

⁷ A. P. Ramirez, A. Hayashi, R. J. Cava, R. Siddharthan, and B. S. Shastry, *Nature* **399**, 333 (1999).

⁸ J. S. Gardner, S. R. Dunsiger, B. D. Gaulin, M. J. P. Gingras, J. E. Greedan, R. F. Kiefl, M. D. Lumsden, W. A. MacFarlane, N. P. Raju, J. E. Sonier, I. Swainson, and Z. Tun, *Phys. Rev. Lett.* **82**, 1012 (1999).

⁹ J. S. Gardner, A. Keren, G. Ehlers, C. Stock, E. Segal, J. M. Roper, B. Fåk, M. B. Stone, P. R. Hammar, D. H. Reich, and B. D. Gaulin, *Phys. Rev. B* **68**, 180401(R) (2003).

¹⁰ L. Yin, J. S. Xia, Y. Takano, N. S. Sullivan, Q. J. Li, and X. F. Sun, *Phys. Rev. Lett.* **110**, 137201 (2013).

¹¹ N. Shannon, O. Sikora, F. Pollmann, K. Penc, and P. Fulde, *Phys. Rev. Lett.* **108**, 067204 (2012).

¹² R. Applegate, N. R. Hayre, R. R. P. Singh, T. Lin, A. G. R. Day, and M. J. P. Gingras, *Phys. Rev. Lett.* **109**, 097205

(2012).

¹³ N. P. Raju, M. Dion, M. J. P. Gingras, T. E. Mason, and J. E. Greedan, *Phys. Rev. B* **59**, 14489 (1999).

¹⁴ J. D. M. Champion, M. J. Harris, P. C. W. Holdsworth, A. S. Wills, G. Balakrishnan, S. T. Bramwell, E. Čížmár, T. Fennell, J. S. Gardner, J. Lago, D. F. McMorrow, M. Orendáč, A. Orendáčová, D. McK. Paul, R. I. Smith, M. T. F. Telling, and A. Wildes, *Phys. Rev. B* **68**, 020401(R) (2003).

¹⁵ C. Fan, Z. Y. Zhao, H. D. Zhou, X. M. Wang, Q. J. Li, F. B. Zhang, X. Zhao, and X. F. Sun, *Phys. Rev. B* **87**, 144404 (2013).

¹⁶ G. Kolland, O. Breunig, M. Valldor, M. Hiertz, J. Frielingsdorf, and T. Lorenz, *Phys. Rev. B* **86**, 060402(R) (2012).

¹⁷ W. H. Toews, S. S. Zhang, K. A. Ross, H. A. Dabkowska, B. D. Gaulin, and R. W. Hill, *Phys. Rev. Lett.* **110**, 217209 (2013).

¹⁸ Q. J. Li, Z. Y. Zhao, C. Fan, F. B. Zhang, H. D. Zhou, X. Zhao, and X. F. Sun, *Phys. Rev. B* **87**, 214408 (2013).

¹⁹ J. R. Stewart, G. Ehlers, A. S. Wills, S. T. Bramwell, and J. S. Gardner, *J. Phys.: Condens. Matter* **16**, L321 (2004).

²⁰ J. D. M. Champion, A. S. Wills, T. Fennell, S. T. Bramwell, J. S. Gardner, and M. A. Green, *Phys. Rev. B* **64**, 140407(R) (2001).

²¹ A. K. Hassan, L. P. Lévy, C. Darie, and P. Strobel, *Phys. Rev. B* **67**, 214432 (2003).

²² J. N. Reimers and A. J. Berlinsky, *Phys. Rev. B* **48**, 9539 (1993).

²³ M. Enjalran and M. J. P. Gingras,

- arXiv:cond-mat/0307152.
- ²⁴ A. P. Ramirez, B. S. Shastry, A. Hayashi, J. J. Krajewski, D. A. Huse, and R. J. Cava, Phys. Rev. Lett. **89**, 067202 (2002).
 - ²⁵ O. A. Petrenko, M. R. Lees, G. Balakrishnan, and D. McK. Paul, Phys. Rev. B **70**, 012402 (2004).
 - ²⁶ V. N. Glazkov, C. Marin, and J. P. Sanchez, J. Phys.: Condens. Matt. **18**, L429 (2006).
 - ²⁷ S. S. Sosin, A. I. Smirnov, L. A. Prozorova, G. Balakrishnan, and M. E. Zhitomirsky, Phys. Rev. B **73**, 212402 (2006).
 - ²⁸ O. A. Petrenko, M. R. Lees, G. Balakrishnan, V. N. Glazkov, and S. S. Sosin, Phys. Rev. B **85**, 180412(R) (2012).
 - ²⁹ P. Dalmas de Réotier, A. Yaouanc, Y. Chapuis, S. H. Curnoe, B. Grenier, E. Ressouche, C. Marin, J. Lago, C. Baines, and S. R. Giblin, Phys. Rev. B **86**, 104424 (2012).
 - ³⁰ J. P. C. Ruff, J. P. Clancy, A. Bourque, M. A. White, M. Ramazanoglu, J. S. Gardner, Y. Qiu, J. R. D. Copley, M. B. Johnson, H. A. Dabkowska, and B. D. Gaulin, Phys. Rev. Lett. **101**, 147205 (2008).
 - ³¹ S. S. Sosin, L. A. Prozorova, M. R. Lees, G. Balakrishnan, and O. A. Petrenko, Phys. Rev. B **82**, 094428 (2010).
 - ³² M. E. Zhitomirsky, M. V. Gvozdkova, P. C. W. Holdsworth, and R. Moessner, Phys. Rev. Lett. **109**, 077204 (2012).
 - ³³ L. Savary, K. A. Ross, B. D. Gaulin, J. P. C. Ruff, and L. Balents, Phys. Rev. Lett. **109**, 167201 (2012).
 - ³⁴ A. Poole, A. S. Wills, and E. Lelièvre-Berna, J. Phys.: Condens. Matt. **19**, 452201 (2007).
 - ³⁵ H. B. Cao, I. Mirebeau, A. Gukasov, P. Bonville, and C. Decorse, Phys. Rev. B **82**, 104431 (2010).
 - ³⁶ S. T. Bramwell, M. J. P. Gingras, and J. N. Reimers, J. Appl. Phys. **75**, 5523 (1994).
 - ³⁷ H. Cao, A. Gukasov, I. Mirebeau, P. Bonville, C. Decorse, and G. Dhalenne, Phys. Rev. Lett. **103**, 056402 (2009).
 - ³⁸ S. R. Dunsiger, R. F. Kiefl, J. A. Chakhalian, J. E. Greedan, W. A. MacFarlane, R. I. Miller, G. D. Morris, A. N. Price, N. P. Raju, and J. E. Sonier, Phys. Rev. B **73**, 172418 (2006).
 - ³⁹ A. Yaouanc, P. Dalmas de Réotier, V. Glazkov, C. Marin, P. Bonville, J. A. Hodges, P. C. M. Gubbens, S. Sakarya, and C. Baines, Phys. Rev. Lett. **95**, 047203 (2005).
 - ⁴⁰ Q. J. Li, L. M. Xu, C. Fan, F. B. Zhang, Y. Y. Lv, B. Ni, Z. Y. Zhao, and X. F. Sun, J. Cryst. Growth **377**, 96 (2013).
 - ⁴¹ X. F. Sun, W. Tao, X. M. Wang, and C. Fan, Phys. Rev. Lett. **102**, 167202 (2009).
 - ⁴² Z. Y. Zhao, X. M. Wang, C. Fan, W. Tao, X. G. Liu, W. P. Ke, F. B. Zhang, X. Zhao, and X. F. Sun, Phys. Rev. B **83**, 014414 (2011).
 - ⁴³ X. M. Wang, C. Fan, Z. Y. Zhao, W. Tao, X. G. Liu, W. P. Ke, X. Zhao, and X. F. Sun, Phys. Rev. B **82**, 094405 (2010).
 - ⁴⁴ X. M. Wang, Z. Y. Zhao, C. Fan, X. G. Liu, Q. J. Li, F. B. Zhang, L. M. Chen, X. Zhao, and X. F. Sun, Phys. Rev. B **86**, 174413 (2012).
 - ⁴⁵ Q. J. Li, Z. Y. Zhao, H. D. Zhou, W. P. Ke, X. M. Wang, C. Fan, X. G. Liu, L. M. Chen, X. Zhao, and X. F. Sun, Phys. Rev. B **85**, 174438 (2012).
 - ⁴⁶ V. N. Glazkov, M. E. Zhitomirsky, A. I. Smirnov, H.-A. Krug von Nidda, A. Loidl, C. Marin, and J.-P. Sanchez, Phys. Rev. B **72**, 020409(R) (2005).
 - ⁴⁷ R. Berman, *Thermal Conduction in Solids* (Oxford University Press, Oxford, 1976).
 - ⁴⁸ P. Bonville, J. A. Hodges, M. Ocio, J. P. Sanchez, P. Vulliet, S. Sosin, and D. Braithwaite, J. Phys.: Condens. Matt. **15**, 7777 (2003).
 - ⁴⁹ X. F. Sun, I. Tsukada, T. Suzuki, S. Komiya, and Y. Ando, Phys. Rev. B **72**, 104501 (2005).
 - ⁵⁰ X. F. Sun, A. A. Taskin, X. Zhao, A. N. Lavrov, and Y. Ando, Phys. Rev. B **77**, 054436 (2008).
 - ⁵¹ L. D. C. Jaubert and P. C. W. Holdsworth, J. Phys.: Condens. Matt. **23**, 164222 (2011).
 - ⁵² C. Hess, B. Büchner, U. Ammerahl, L. Colonescu, F. Heidrich-Meisner, W. Brenig, and A. Revcolevschi, Phys. Rev. Lett. **90**, 197002 (2003).
 - ⁵³ C. Hess, Eur. Phys. J. Special Topics **151**, 73 (2007).
 - ⁵⁴ A. V. Sologubenko, T. Lorenz, H. R. Ott, and A. Freimuth, J. Low Temp. Phys. **147**, 387 (2007).